

Final Design Report

Preston Gomersall, Benjamin Arena, Ryan Banh, Daniel Johnson, Brendan Liang

Executive Summary

We have constructed our senior project with the primary objective of designing and building an RC aircraft that maximizes the given scoring function:

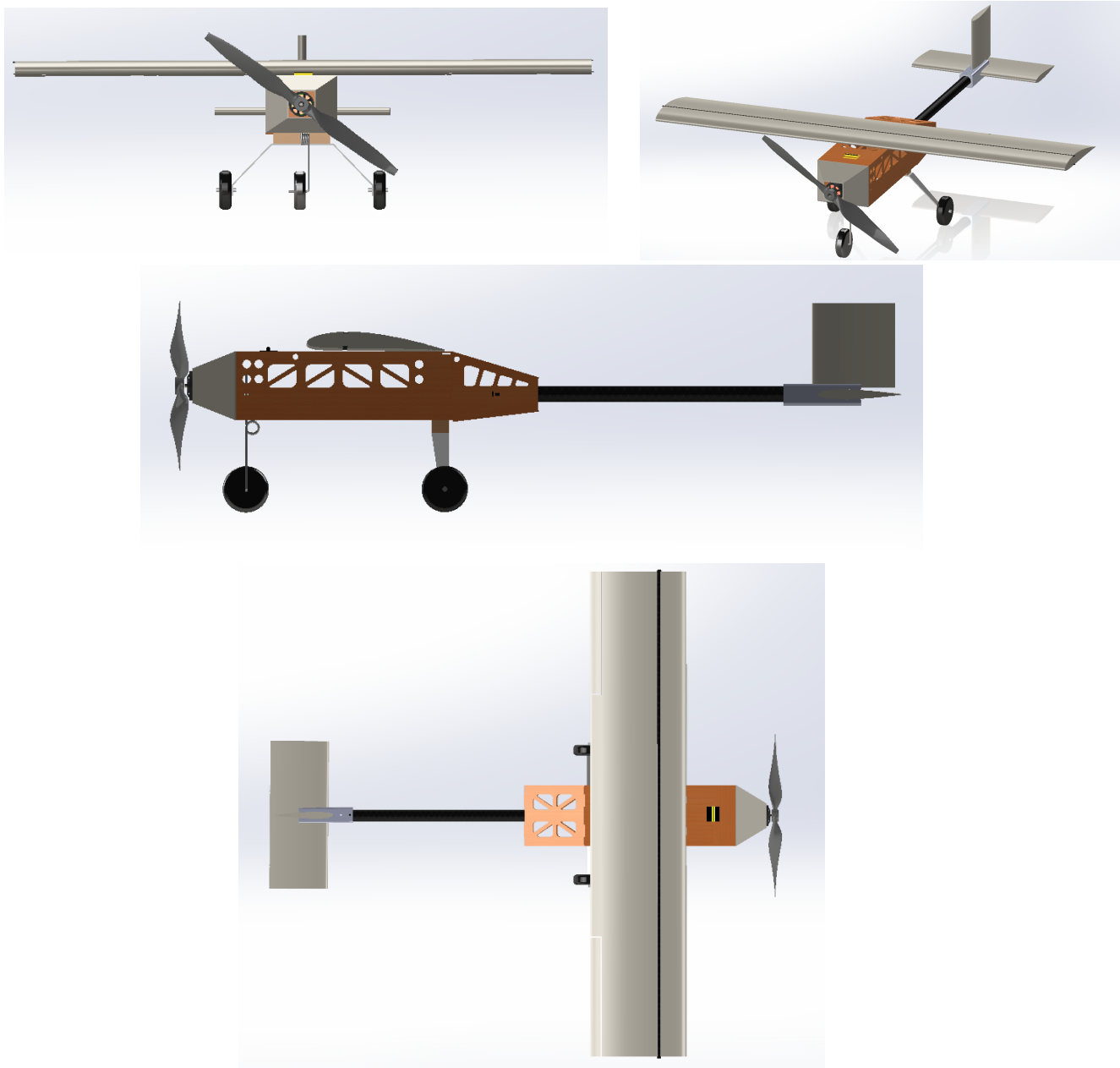
$$Score = 7.5 \frac{W_p}{W_r} + f + \frac{V_{max}}{V_r} + 7.5B$$

This scoring function served as our guide in setting a clear goal for our senior project. We considered various factors such as gross weight, payload weight, maximum velocity, and stability when adding or removing payload. Through careful analysis of this scoring function, we were able to design an airplane that performed well and achieved high scores.

We were provided with specific components such as the battery and motor, which helped narrow down our design to meet their specifications. We then utilized our knowledge from previous classes, including propulsion, aerodynamics, structural engineering, fluid mechanics, and aerospace design to analyze the aircraft thoroughly. The results of our analysis are presented in the following 19 pages of this report. By considering all these factors and applying our expertise, we successfully designed and manufactured an RC aircraft that met our goals. Below is a picture of our finished aircraft and on the next page is a detailed CAD drawing of the plane



High-Level CAD



Gantt Chart

Presented below is our planned schedule that we followed for the final design and fabrication stages of our RC aircraft. The separate fabrication of the fuselage and main wing took roughly a week longer than expected due to various design changes and fabrication errors. However, much of the time was made up on the programming and attaching of the servo and control surfaces and ultimately we completed our first ground roll test a week ahead of schedule; This allowed us to complete a second groundroll test and make more significant improvements and reinforcements to the aircraft structures.

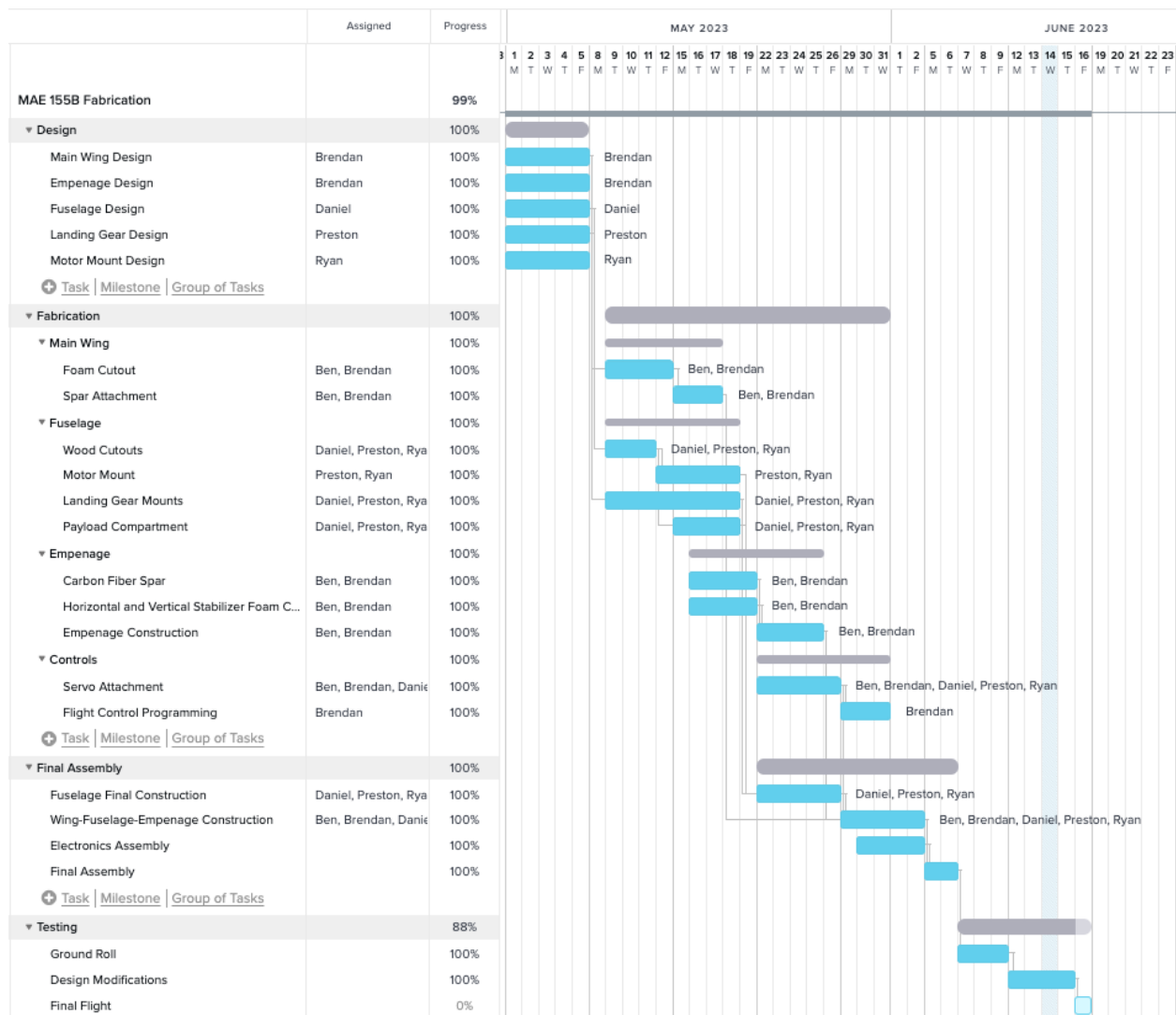


Table of Contents

Executive Summary	1
High-Level CAD	2
Gantt Chart	2
Table of Contents	4
Conceptual Design	5
Mission Requirements	5
Scoring Analysis	6
Design Requirements	8
Configuration Selection	8
Component Configuration	9
Initial Sizing	9
Preliminary Design	10
Propulsion	10
Aerodynamics	12
Performance	14
Weights & Balance	15
Future Work	16
Detailed Design	17
Fuselage Construction	17
Tail And Wing Construction	19
Testing	20
References	21

Conceptual Design

Mission Requirements

To meet our mission requirements, we began by thoroughly analyzing the fly space we intended to traverse. We used Google Maps to establish the boundaries of the fly area, obtaining a rough estimate of the fly field and creating a mission profile from that information. Figure 1 displays the printed map of the fly field, which also includes the flight path for our RC aircraft.

Our mission objective is to complete two laps around the perimeter of the fly field. We initiate the mission by taking off along the runway and aim to have a takeoff as soon as we reach the minimum velocity for stall. Following this, the RC aircraft will travel to a height of 15.24 meters over a distance of 100 meters, providing us with a climb angle of approximately 8.69° and a value of $G = 0.151$.

Once the aircraft reaches the desired altitude, we will execute a steady level turn maneuver with a bank radius of 25 m, giving us a rough estimate of the load factor on the plane. Using some basic equations we found our load factor to be $n = 1.55$ with the bank angle of approximately 50° during this maneuver. The RC aircraft will continue to navigate around the field at steady level flight until it reaches the runway, where it will perform a touch and go maneuver. The second lap of the mission will be the same as the first, with the addition of a maximum throttle limit test.

Image 1



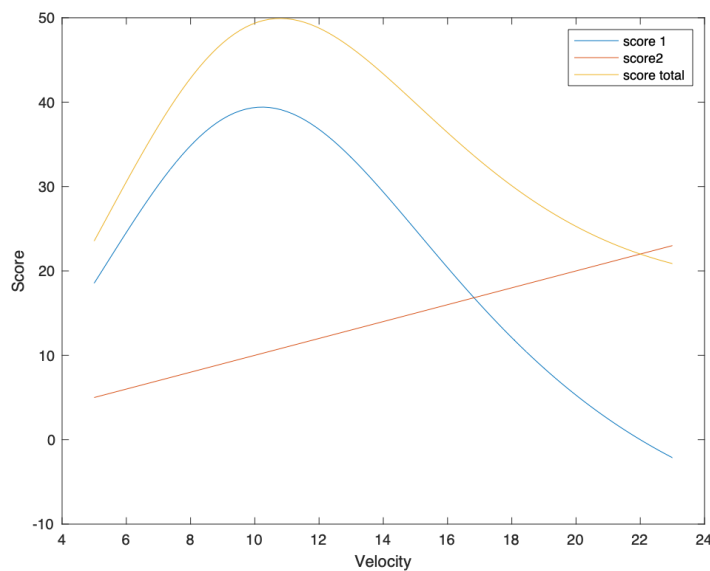
Scoring Analysis

$$Score = 7.5 \frac{W_p}{W_r} + f + \frac{V_{max}}{V_r} + 7.5B$$

To begin our analysis, we examined the scoring function presented above. Initially, we found that two of the parameters had negligible impact on our analysis: the points awarded for the ability to fly at different payloads and the payload fraction. Therefore, we focused our attention on the remaining scoring parameters.

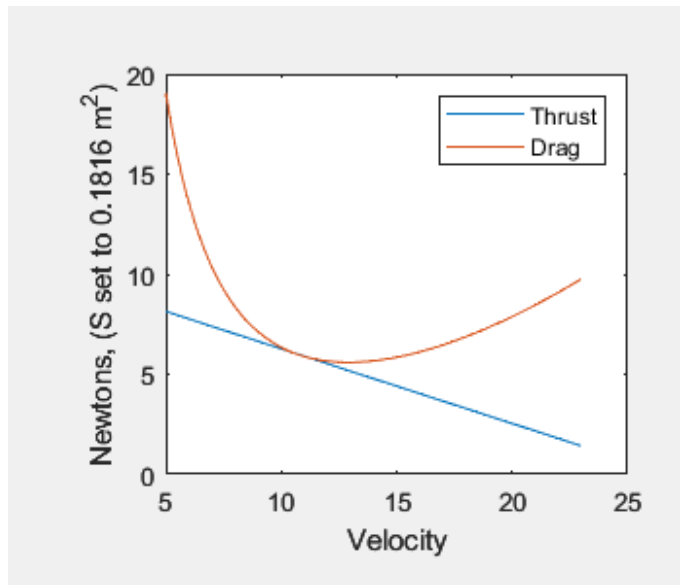
To analyze these parameters, we converted them into functions of velocity and plotted them in figure 1. To do this, we had to estimate values for important design parameters such as wing loading, aspect ratio, Oswald efficiency, and payload fraction. We arrived at these estimates by drawing on our knowledge of other RC aircraft and resources available online.

Figure 1



Using this analysis, we identified an optimal weight of 1.77kg to maximize the scoring function. However, our actual aircraft weight is slightly lower at 1.27kg. We reduced the weight from the optimal value because we observed in the graph below that the plane would only be able to fly at one specific flying condition. To address this limitation, we reduced the planform area of the wing, which in turn reduced the drag but also lowered our gross weight due to our assumed wing loading.

Figure 2



Design Requirements

To accomplish the goal of carrying a payload of golfballs in an RC aircraft designed to maximize the score, it was clear that it was important to increase the payload weight fraction while keeping the internal volume large enough to fit the balls. As a result, the weight of the materials making up the airplane are a major consideration when creating the design for the airplane.

Additionally, another requirement that needed to be met was ease of manufacturing since the RC airplane would be built by hand. It can be reasonably assumed that spare parts or multiple versions of the same component would need to be manufactured as well during the fabrication phase, requiring a design that was quick to reproduce and modify. While the weight requirements influenced the material selection, the requirement that it needed to be built and flown greatly influenced the structure and configuration.

Configuration Selection

In the beginning stages of development of our RC aircraft, we evaluated various wing configurations based on factors such as stability, control, maneuverability, lift-to-drag ratio, weight, and complexity. Using a Pugh chart, we narrowed down our options to three designs: Tandem Wing, Flying Wing, and Standard Untapered Wing. Each parameter is measured on a scale from 3 being optimal and -3 being a subpar design choice.

While the Tandem Wing offered superior stability and control, it would require us to design and manufacture two wings, adding to the complexity. The Flying Wing showed promise in terms of

aerodynamics and speed, but ultimately we decided to go with the Standard Untapered Wing design. This option is relatively stable, easy to control, and most importantly, it simplifies the design and manufacturing process.

Our main goal for this project is to produce a simple and efficient aircraft, so that we can accelerate the manufacturing and testing process. With this in mind, we believe that the Standard Untapered Wing design is the best choice for our needs.

Table 1

Design	Stability	Control	Maneuverability	Lift-to-drag ratio	Weight	Complexity	Total
Control Canard	2	2	1	1	-1	-1	4
Lifting-Canard	2	1	2	2	-2	-1	4
Tandem Wing	3	3	2	2	-2	-2	6
Three-Surface Aft-Strake	2	2	2	1	-1	-1	5
Tailless	-2	-2	-1	1	1	0	-3
Flying Wing	0	1	2	3	2	-1	7
Droop Wing Outer Panels	0	0	1	1	0	0	2
Winglets weight **	1	1	0	2	0	-1	3
Standard Untapered Wing	2	2	1	1	0	1	7

Component Configuration

To strike a balance between complexity, reliability, and performance, we carefully considered various options for our component configuration. To aid in our decision-making process, we constructed a Pugh chart that allowed us to compare and contrast the advantages and disadvantages of different materials, including foam, balsa wood, and 3D-printed parts. After analyzing the chart, we concluded that the best choice for our fuselage was a combination of wood and monokote material, as it offered the necessary structural rigidity. Meanwhile, for the wings, we opted for hollow foam despite its slightly lower score, we determined that it could be easily laser-cut and hollowed out with a hot wire. Additionally, using the laser cutter for the wings will allow us to produce multiple copies with precision, which could prove useful in case of an accident.

Table 2

Material	Hallowed Foam	Wood/Monokote	3D-Printed	Importance Multiplier	Range Max	Range Min
Ease of Manufacturing	3	1.5	-1.5			
Taper	1.5	2.25	2.25	1.5	3	-3
Weight	1.5	3	0			
Modularity	1.5	0	-1.5	1		
Repairability	0.5	1.5	-1.5	0.5		
Sum	8	8.625	-3.375			

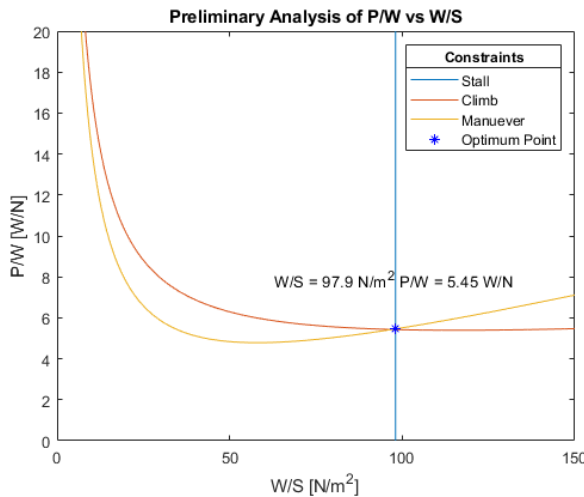
Initial Sizing

Using values gathered from the scoring and aerodynamics analysis we were able to get an estimate for the sizing of the plane. Some of the values we used for sizing are given below:

$$V_{stall} = 11 \text{ m/s}, G = 0.13333, \eta = 0.8, C_{L,max} = 1.3, n = 2, C_{D0} = 0.0311 \text{ and } V = 18 \text{ m/s}$$

These assumptions gave the following Power to Weight (P/W) verse Weight to wing area (W/S) ratios, described in the graph below.

Figure 3



From this we see an initial estimate for wing loading $W/S = 97.9 \text{ N/m}^2$ and power ratio of $P/W = 5.45 \text{ W/N}$. This gave us a good initial guess to plug into the scoring function for W/S and gives us useful information on the power to weight ratio which the scoring function analysis does not give accurately.

From the scoring function, the gross weight was calculated to be 17.38 N or 1.77 kg. Using this result, some initial sizing can be calculated. Aside from the wing loading, and gross weight, the payload weight, power to weight ratio and wing area can be estimated:

$$\begin{aligned} \text{Gross Weight} &= 17.38 \text{ N} \\ \text{Payload Weight} &= 6.48 \text{ N} \\ \text{Wing Loading} &= 97.9 \text{ N/m}^2 \end{aligned}$$

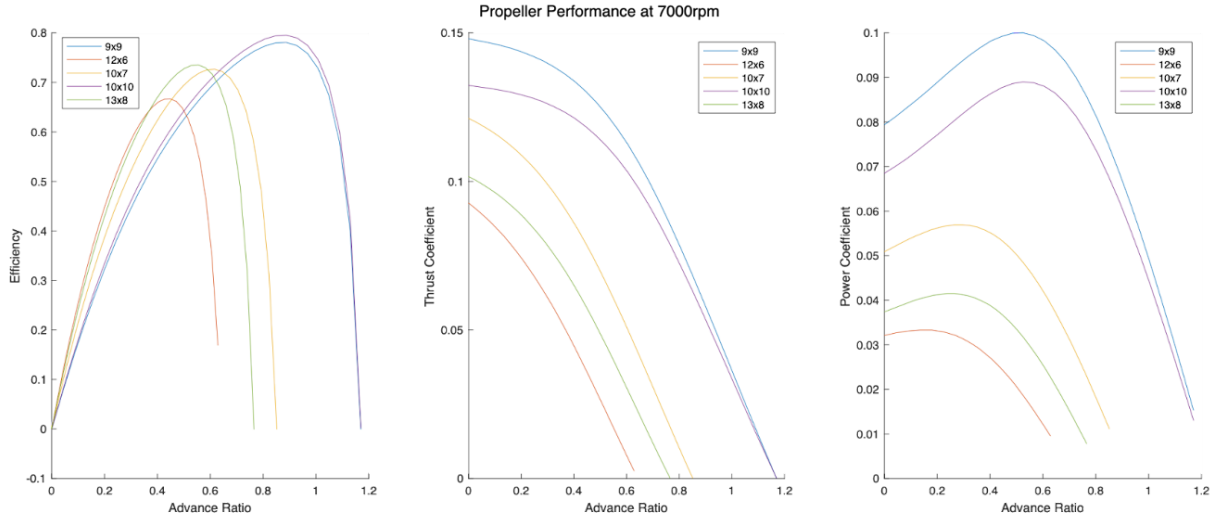
Preliminary Design

Propulsion

The analysis of our propulsion system relied heavily on several key factors, including the specific motor provided to us (Cobra C-2217/16), the available propellers in our lab, and the expected velocities of our plane during flight. Based on our calculations from aerodynamics, we anticipated that the cruise speed would fall within a range of approximately 15 m/s to 20 m/s. Using this information, we calculated that the Advance Ratio would likely range from 0.35 to 0.65, depending on the blade diameter. Our analysis determined that the 10x7E propeller offered the most efficient performance across this range of ratios as seen in the graphs below.

At a cruise of 15 m/s, the 10x7E propeller can produce roughly 4.7 N of thrust with a takeoff thrust of roughly 6.4 N at 7000 RPM, a value roughly in line with the Cobra C2217/16 Motor data for the specified propeller. This produces a torque of 0.158 N-m and 0.14 N-m and a power of 116.1 W and 102.8 W at take off and cruise respectively.

Figure 4



Aerodynamics

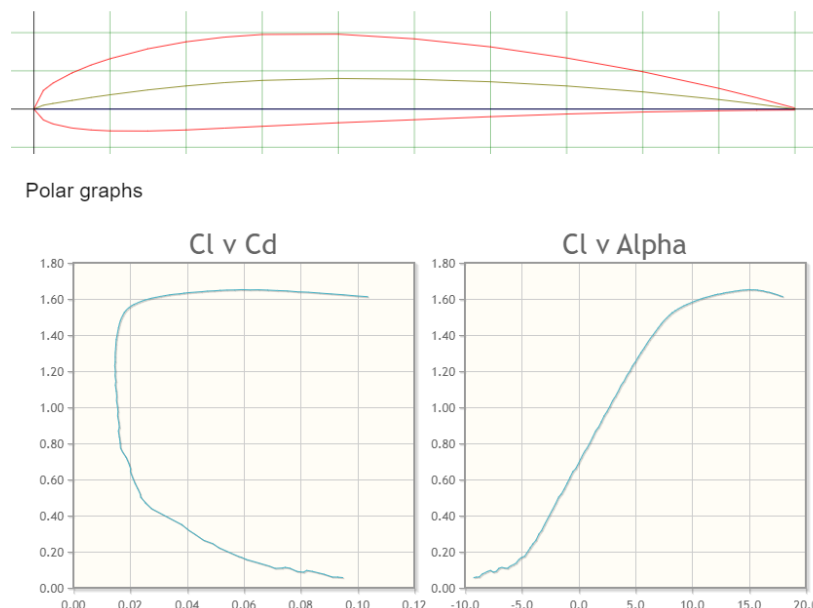
After careful consideration of various factors, including a Reynolds number of 2.24×10^5 , a mach number of 0.05, as well as thickness and camber requirements, we decided to select the ideal airfoil for our project. Our initial choice was the DAE-31 airfoil, which had favorable camber properties, particularly useful for generating lift at low speeds. However, this airfoil was primarily designed for higher mach numbers and transonic flow, leading us to explore alternative options.

Ultimately, we opted for a NACA airfoil, specifically the NACA 4412 as depicted below. This choice was influenced by our plans to laser cut the airfoil, with a NACA airfoil potentially simplifying the manufacturing process. Additionally, the NACA 4412 is an excellent choice for low mach number and Reynolds numbers, as supported by the accompanying drag polar and C_L vs. Alpha curves.

Figure 5

NACA 4412 (naca4412-il)

NACA 4412 - NACA 4412 airfoil

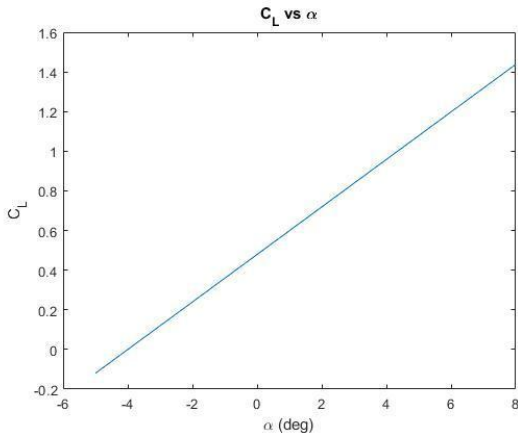


From the polar graph charts we were able to find the 3-D lift coefficients C_{L_a} and $C_{L,\max}$ which were found to be:

$$C_{L_a} = .1198 \text{ and } C_{L,\max} = 1.3230$$

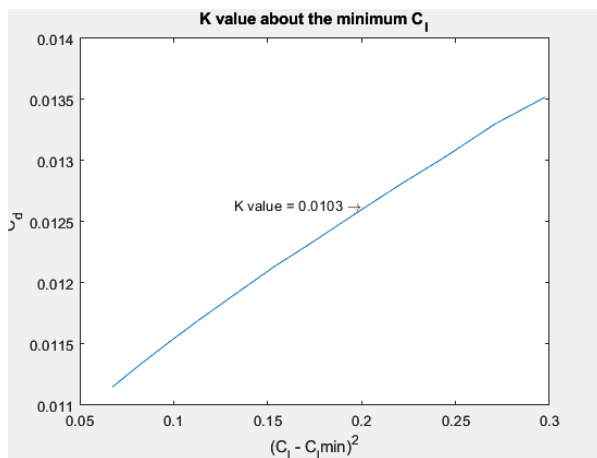
Using these values we were able to plot our own C_L vs alpha curve which is provided below:

Figure 6



Our next step in the process was to determine the K value for our airfoil. This value is dependent on both the form drag and profile drag of the airfoil that we picked. To determine this value we calculated the minimum drag based on the polar charts and plotted a $(Cl - Cl_{min})^2$ vs cd graph.

Figure 7



Then the drag buildup method was used to find C_{Dmin} so that we can find C_D . The parasitic drag breakdown is given below:

Table 3

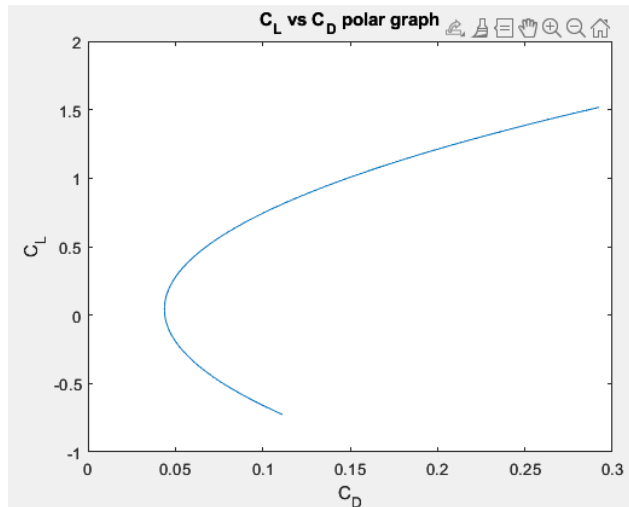
Component	C_{D0}
Wing	.0114
Horizontal Tail	.0025
Vertical Tail	.0013

Fuselage	.0155
Motor	.0001
Landing Gear	.0003
Total	.0311

We ended up calculating a value of $C_D = 0.0417$ for the coefficient of drag at cruise conditions.

From this we were able to get a lift to drag ratio at cruise flight. We got a lift to drag ratio of 5.0511. At this point of maximum efficiency we calculated we only need to use 20% of the max throttle. We were able to plot C_L Vs C_D graph.

Figure 8



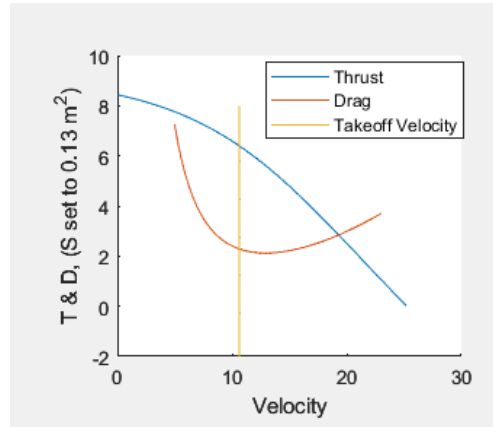
Performance

The performance of our aircraft is heavily reliant on two factors: the thrust-to-drag ratio during flight and the lift-to-drag ratio during cruise flight. Through our comprehensive data analysis, we were able to determine the optimal thrust of our aircraft using the data provided for our propeller (10X7E). Upon reaching 7000 rpm, our propeller can generate a maximum thrust of 8.5 newtons at zero thrust.

By plotting this data in figure 9, along with our drag build-up method, as outlined in our aerodynamics section, we can pinpoint our takeoff speed, represented by a vertical line on the graph. This value is equal to 80 percent of our max coefficient of lift, as we aim to avoid stalling

the plane during takeoff. With these calculations, we have determined the range of velocities at which our thrust exceeds drag, allowing us to travel at speeds ranging from 10.5m/s to 19.5 m/s.

Figure 9



Moreover, we have analyzed our lift-to-drag ratio during steady level flight and found it to be 7.3, which is on the higher side for most RC aircraft. This finding is reassuring as it validates our choice in airfoil design for our aircraft. With our combined knowledge of these critical ratios, we can ensure that our aircraft operates at peak performance levels.

Weights & Balance

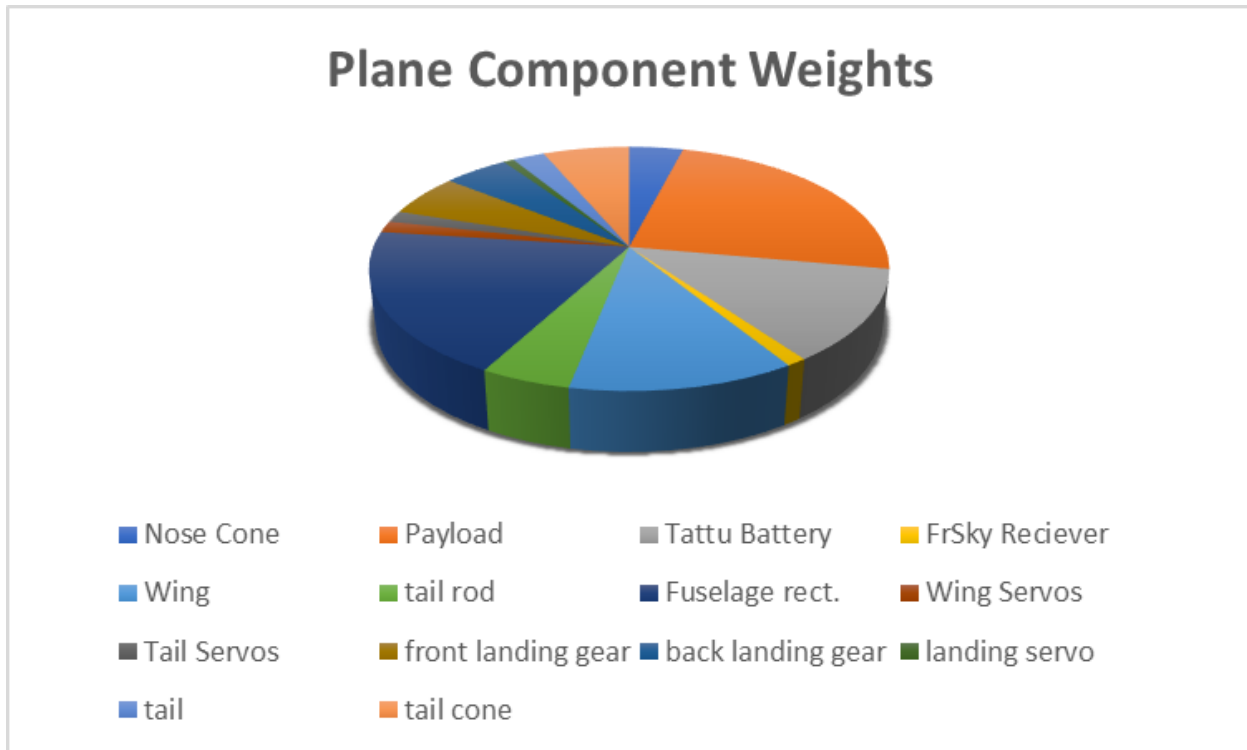
Another critical aspect of our aircraft design was the determination of its weight. We utilized our scoring function to estimate the gross weight and payload-to-weight fraction, which were calculated to be 1.27kg and 0.3, respectively. However, it was equally important to ensure that our aircraft's geometry matched these weight specifications.

Initially, we measured the weight of some components in the lab, such as the battery, receiver, motor, controller, and landing gear. Additionally, the payload fraction allowed us to determine the payload weight, which was 8 golf balls. The remaining weights were determined by calculating densities and volumes, utilizing Solidworks to calculate the weight for various materials. After we constructed the plane we were able to accurately measure the weights using a scale and those values are represented in the figure below.

After determining the weights in figure 10, we identified locations along the fuselage where these weights would act and determined the center of gravity. We also calculated the center of gravity by balancing the plane along the wing tips after the plane is constructed. The neutral point was calculated using the coefficients of lifts and planform areas for the tail and wing. We chose to disregard the fuselage in our aerodynamic center calculation because it was challenging

to determine for a box fuselage, and we estimated that the contribution to the overall calculation would be insignificant. Utilizing the center of gravity and aerodynamic center, we calculated a static margin of 15.53.

Figure 10



Aerodynamic center	Static Margin	C.G
21.19439841	15.53448125	18.70121

Future Work

Before we start the manufacturing of the plane, we plan to go through our calculations again and check for any areas that could still be improved for our design. We also still need to conduct a structural analysis for the plane to make sure that the materials we chose can handle the loads the plane will experience. We also plan to do a dynamically stability test and calculate the moments of inertia for the plane. The weights and positioning of components are still preliminary and those will be moving around throughout the design.

Detailed Design

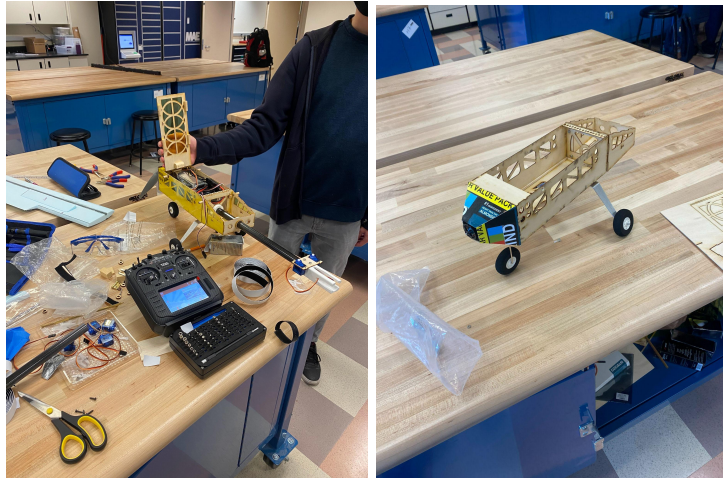
After finalizing the dimensions of our aircraft, we embarked on the construction phase of our design. To streamline our workflow, our team of five individuals was divided into two specialized sections. Three of us focused on the construction of the fuselage, while the remaining two dedicated their efforts to crafting the wings and tail.

Fuselage Construction

The image below showcases the completed fuselage, serving as a visual reference. Our decision to employ basswood for the outer frame of the fuselage was driven by its exceptional combination of strength and lightweight properties. We carefully deliberated on alternatives such as balsa wood, but its inherent flimsiness rendered it unsuitable for withstanding the various loads that our aircraft would endure.

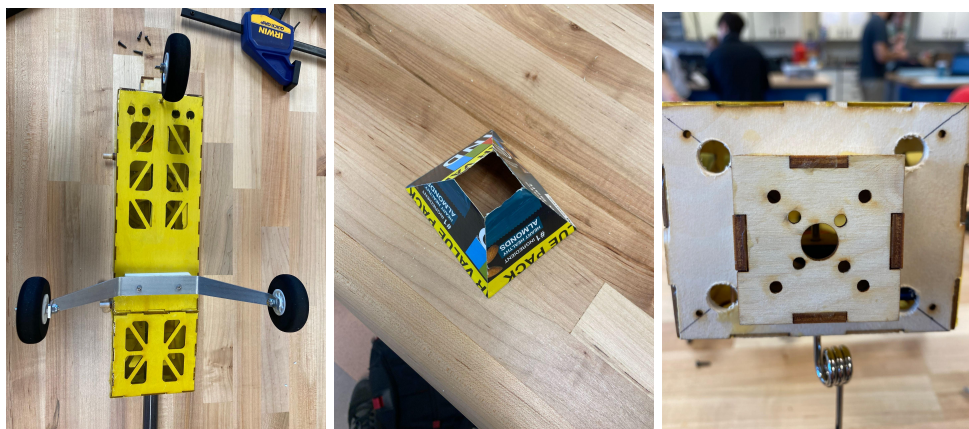
To design the fuselage of the plane we utilized AutoCAD and then laser cut the pieces in the UCSD Aerospace Fabrication Lab. The rectangular pieces were skillfully assembled, securing the edges with a puzzle piece design and wood glue. Enhancing the versatility of our fuselage, we incorporated a hinged top (depicted in figure 11 below), which facilitates convenient payload installation, removal, as well as access to the avionics systems. This hinged top is firmly affixed to the sidewall of the plane through the use of nuts and bolts, thereby imparting superior torsional and bending stiffness during flight operations.

Figure 11



The front section of the fuselage plays a crucial role as it accommodates the motor mount, as depicted in figure 12. Our team opted for a thicker piece of wood for this mount because this component of the plane will endure the highest loads from our propeller. The motor can be removed and screwed back in through an access hole on the inside of the fuselage. The nose cone of the plane is glued to the front end of the fuselage and ensures a more streamlined fuselage configuration.

Figure 12



The landing gear played a crucial role in our fuselage construction, providing essential support for our aircraft. Figure 13 showcases our landing gear design, featuring strategically drilled holes on the underside of the fuselage. We opted for a tricycle configuration for simplified takeoff and landing, although we did consider a tail dragger design for better performance on rough terrain. To ensure even alignment, we utilized a spacer to level the back landing gear with the front gear. Additionally, we implemented a dedicated mount inside the fuselage for the front landing gear, minimizing turbulence during takeoff. This mount also accommodates a servo for precise steering control during takeoff.

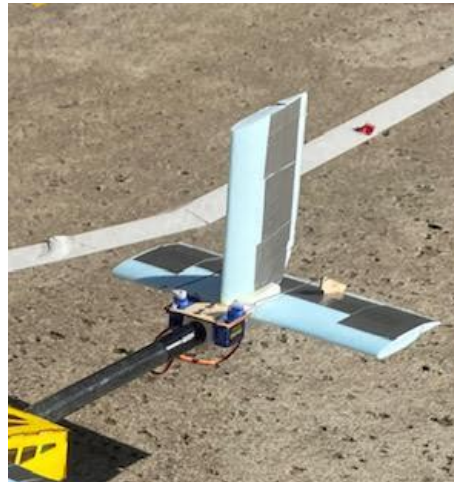
Tail And Wing Construction

In our design, we incorporated a tail rod that extends from the rear of the fuselage to the tail of the aircraft, as depicted in figure 14. Instead of elongating the fuselage all the way to the tail, we opted for a weight-saving measure by utilizing the tail rod. Carefully determining the dimensions, we sized the fuselage to accommodate our payload of 8 golf balls and electronics, striking an optimal balance between capacity and weight.

To secure the tail rod to the fuselage, we employed clamps and fastened them with nuts and bolts. At the end of the tail rod, a 3D printed mounting piece was attached, serving as a platform for connecting the horizontal and vertical stabilizers. Additionally, this mount features a laser cut component for housing the servos, enabling precise control over the elevator and rudder.

Completing the attachment to the fuselage are the horizontal and vertical stabilizers. These vital components are securely glued to a 3D printed tail mount, as showcased in figure 14. Initially, we designed the control surfaces based on the dimensions of our tail. However, to enhance maneuverability and stability during flight, we made the decision to increase the span and chord length of the stabilizers, ultimately refining the performance of our aircraft.

Figure 14



The wing construction involved precision cutting of foam using the laser cutter available in the design and fabrication lab. Our team opted to use foam material versus a wood constructed wing because of its lightweight and easy manufacturability. By generating a g-code specific to the NACA airfoil we selected, the laser cutter skillfully shaped our wing to desired specifications.

To enhance the structural integrity of the wing, the installation of spars was essential. We inserted two carbon fiber spars along the top and bottom of the wing at the quarter chord. The spars on the top and bottom of the wing act as an I-Beam for the wing and provide an extreme amount of stiffness.

Using the Dremel, we also cut out holes in the wing for the servos to allow for a flush design, reducing drag. These servos allow us to control the ailerons of the plane so that we can maneuver the plane during flight. The ailerons were tested using the transmitter and receiver in class and

trimmed to be level at the neutral position. A finished product of our wing is shown in figure 14 below.

Figure 15



Testing

Following the completion of our plane's construction and assembly, a series of tests were conducted to ensure the plane's reliability on fly day. We first completed a ground roll test outside the EBU 2 building. During this test, we encountered an unexpected setback—the front landing gear snapped off. Promptly responding to this issue, we engineered a more robust and resilient front landing gear design, specifically tailored to withstand the challenging terrain of the mission bay fly field. Figure 16 captures a picture of the plane during the ground roll test.

Furthermore, we assessed the motor's performance to prevent overheating during flight operations. To achieve this, we conducted tests by running the motor at full throttle while keeping the propeller off. The slight gaps between the motor and nose cone allow for air to flow in and out of the nose cone, having a convective effect. Although this may marginally contribute to aerodynamic drag, it crucially enables effective motor cooling.

Lastly, our team conducted a comprehensive drop test to assess the plane's landing capabilities. Equipped with our newly installed landing gear, we carefully released the aircraft from a waist-high position. The primary objective of this test was to verify whether the plane could sustain a landing without causing any damage to the fuselage and avoiding any potential crashes. Although our plane lacked suspension, we were pleased to witness that both the landing gear and fuselage remained intact.

References

Cobra C2217/16 Motor Propeller Data. Innov8tive designs homepage. (n.d.). Retrieved April 28, 2023, from https://www.innov8tivedesigns.com/images/specs/Cobra_2217-16_Specs.htm

APC Propellers. (2023, March 8). *Performance data.* APC Propellers. Retrieved April 28, 2023, from <https://www.apcprop.com/technical-information/performance-data>

